Solid Freeform Fabrication 2024: Proceedings of the 35th Annual International Solid Freeform Fabrication Symposium – An Additive Manufacturing Conference
Reviewed Paper

CRACK GROWTH AND FATIGUE-LIFE PREDICTIONS FOR Ti-6Al-4V FABRICATED VIA LASER DIRECTED ENERGY DEPOSITION

Leah Buiter[1], Aref Yadollahi[1*], and James C. Newman, Jr.[2]

[1] Department of Mechanical and Civil Engineering, Purdue University Northwest, Hammond, IN 46326

[2] Department of Aerospace Engineering, Mississippi State University, Mississippi State, MS 39762

[*]Corresponding Author, Phone: (219) 989-3147, e-mail: arefy@pnw.edu

Abstract

This study investigates the fatigue-crack-growth and fatigue-life behaviors of Ti-6Al-4V fabricated via laser-based directed energy deposition. Crack-growth rate data were obtained over a wide range of stress ratios, covering crack growth rates from near-threshold to fracture. Uniaxial fatigue tests were conducted on both notched and unnotched specimens under constant-amplitude loading with stress ratio of R = 0.1. A plasticity-induced crack closure model, FASTRAN, was employed to predict the fatigue life of these specimens based on the size of process-induced defects detected via X-ray computed tomography. The fatigue-life prediction results, along with comparisons to experimental fatigue data and fractographic analysis of the fracture surfaces, highlight the critical importance of accounting for multi-site crack growth in accurately assessing the fatigue-life of AM materials. Neglecting the effect of multi-crack growth and coalescence leads to an overestimation of fatigue life, particularly in the short- and mid-life regimes.

Keywords: Additive manufacturing; FASTRAN; Crack closure; Small-crack growth

Introduction

Additive manufacturing (AM) has transformed advanced manufacturing processes, enabling the production of complex geometries and highly customized components with precision across industries such as aerospace, healthcare, and energy. In particular, metal AM offers the ability to create complex shapes — previously impossible or prohibitively expensive using traditional methods — along with advantages like customization, reduced lead times, and part consolidation. However, alongside these advancements arise new challenges, particularly in the areas of qualification and certification, where ensuring the consistent performance, reliability, and structural integrity of AM components under diverse and demanding service conditions becomes critical [1]. The layer-by-layer deposition process and the complex thermal cycling inherent to metal AM lead to unique microstructural characteristics that differ significantly from those in conventionally manufactured materials. This microstructural complexity, combined with the random nature of process-induced defects, introduces significant uncertainty in predicting the performance of AM components under service loading conditions. As AM technology is increasingly adopted for critical, high-performance applications, the need to fully understand the process-structure-property-performance relationships becomes crucial. By unraveling these intricate relationships, we can unlock the full potential of AM, ensuring its components meet the stringent demands of reliability and longevity in mission-critical applications [1-3].

The static mechanical properties of AM materials, including tensile strength and hardness, are often comparable to or even surpass those of conventionally manufactured counterparts [2]. However, the inherent complexities of the AM process — such as microstructural heterogeneity, residual stresses from rapid thermal cycling, and the presence of process-induced defects like gas pores and lack of fusion (LOF) — introduce significant uncertainty and variability in mechanical performance [1,2]. These factors become particularly critical in fatigue-sensitive applications. Defects act as stress concentrators, accelerating crack initiation and growth, resulting in inferior performance under cyclic loading compared to traditionally manufactured metals. In particular, AM metals tend to exhibit shorter fatigue lives, reduced crack growth resistance, and increased scatter in fatigue data due to the unpredictable nature of defect distribution and microstructural anisotropy. This variability is further compounded by residual stresses that can alter local stress fields and fatigue-crack-growth paths. Consequently, the reduced reliability and increased variability under cyclic loading remain key obstacles to the widespread adoption of metal AM, especially in high-stakes applications such as aerospace, where the consequences of material failure can be catastrophic [1-4].

In order to achieve accurate fatigue-life predictions, an understanding of the fatigue-crack-growth behavior is needed. Accurate representation of fatigue-crack thresholds, i.e., the region where crack growth is either exceedingly slow or nonexistent, is an integral part of reliable fatigue-life predictions. Small cracks, typically characterized by crack lengths below a critical threshold, contribute significantly to the initiation and early stages of fatigue failure [5]. Several investigations have indicated that AM materials display notably lower threshold stress intensity range values in comparison to materials produced through conventional methods [5-8]. This study investigates the fatigue life, along with the small- and large-crack growth behavior, of Ti-6Al-4V specimens fabricated using laser-based directed energy deposition (DED-LB). Ti-6Al-4V was specifically selected due to its extensive use in critical industries such as aerospace, energy, and biomedical, where its superior strength-to-weight ratio, corrosion resistance, and biocompatibility are essential. The alloy's broad application in metal AM, particularly in powder-based techniques, further emphasizes the importance of this research. Gaining a deeper understanding of the fatigue performance of AM Ti-6Al-4V is crucial for advancing its adoption in high-performance industrial applications [9]. By comparing the fatigue-crack-growth and fatigue-life behaviors of AM Ti-6Al-4V with their conventionally manufactured counterparts, this research aims to provide insights into the performance of AM materials under cyclic loading conditions, eventually enabling the further adoption of AM components in mission-critical applications.

Experimental Procedure

In this study, three types of test specimens were fabricated to investigate fatigue life, small-crack growth, and large-crack growth behaviors: (i) standard compact tension, C(T), (ii) single-edge-notch-bend, SEN(B), and (iii) flat $K_T = 1$ dogbone specimens. The dimensions of these specimens, along with the arrangement of the samples on the build plate, are shown in Figure 1. A total of six SEN(B) specimens, six C(T) specimens, and eighteen KT = 1 specimens were fabricated. The SEN(B) and KT = 1 specimens were produced in blocks, with six samples per build plate, while the C(T) specimens were printed with only three samples per build plate due to space limitations. All samples were fabricated in a vertical orientation using an alternating 0-90 degree scanning pattern via a DED-LB system (Optomec LENS 750), utilizing virgin plasma-

atomized Ti-6Al-4V powder. The process parameters chosen were a laser power of 750 W, scanning speed of 1,016 mm/s, and layer thickness and hatching pitch of 508 μm. After fabrication, all specimens were annealed for 1 hour at 760°C in an inert argon atmosphere, followed by air cooling. This process minimizes residual stress and microstructural heterogeneities resulting from part geometry and orientation [10]. The specimens were then extracted from the heat-treated blocks using electrical discharge machining (EDM) to achieve their final geometry and dimensions, in accordance with the relevant ASTM standards [11,12]. Prior to testing, the specimens were examined using X-ray computed tomography. This process of nondestructive analysis enables the visualization and qualification of process-induced defects.

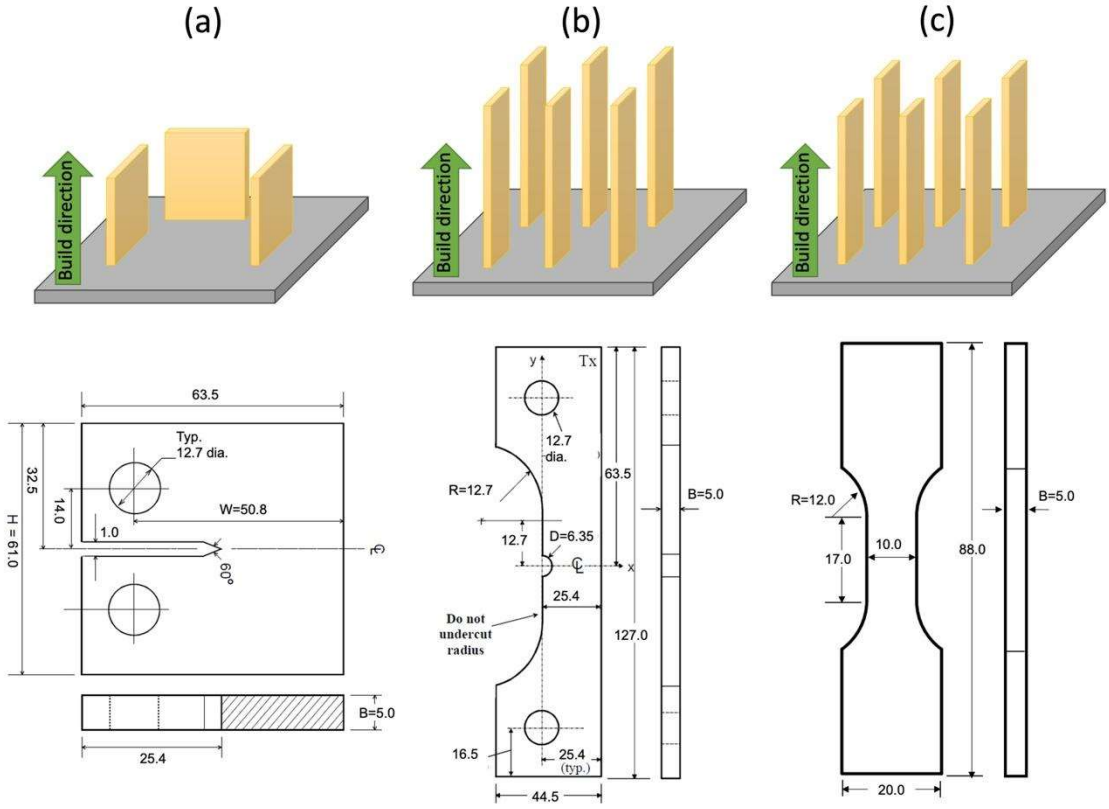

Figure 1. The isometric view of the samples on the build plate and geometry and dimensions of (a) C(T), (b) SEN(B), and (c) $K_T = 1$ fatigue specimens.

The C(T) specimen was used for generating large-crack-growth-rate data, the SEN(B) specimen served as a fatigue and small-crack-growth specimen with a high stress-concentration factor, and the $K_T = 1$ specimen was used for fatigue testing to generate stress-life (S-N) behavior. Uniaxial fatigue tests were performed on the $K_T = 1$ specimens under force-controlled mode (R = 0.1) in accordance with ASTM E466 [11]. Fatigue testing was continued until either failure occurred or 10^7 cycles were reached, at which the test was considered a 'run-out.' Fatigue tests were conducted on SEN(B) specimens under constant amplitude loading of R = 0.1 (it should be noted that compression loads were not allowed on SEN(B) specimens). The large-crack growth tests were conducted on C(T) specimens over a wide range of stress ratios (R = 0.1, 0.4, and 0.7) and produced crack growth rates from near-threshold to fracture. To generate data in the near-

threshold regime, all the specimens were pre-cracked under constant-amplitude compression–compression loading (R = 22 or 40) for about 38,000 cycles. Back-face strain gauges were used during testing of C(T) and SEN(B) to generate crack growth rate data. All testing was performed using a servo-hydraulic load frame under laboratory air condition. Data from small- and large-crack growth tests, previously produced as part of a U.S. Federal Aviation Administration contract with Mississippi State University, are presented alongside the data collected in this study to provide comparison between wrought and AM Ti-6Al-4V [13,14].

Results and Discussion

The results of X-ray computed tomography (XCT), which provide a detailed assessment of process-induced defects are summarized in Table 1. It is worth noting that the C(T) specimens had the highest count of detected defects; approximately three to four times higher than that of the K_T = 1 or SEN(B) specimens. Since all samples were fabricated under identical processing conditions, these differences are likely attributed to geometric variations between the specimens, which influenced the thermal history and promoted defect formation during solidification. Additionally, microstructural analysis was conducted using scanning electron microscopy (SEM). This analysis revealed that the post-fabrication annealing treatment transformed initially α′ martensite phase into the balanced α+β phases. The resulting microstructural characteristics, including phase distribution and morphology, were consistent across all specimen types, indicating that the thermal treatment effectively homogenized the microstructure, despite the differences in defect distribution.

Table 1. Summary of nondestructive defect analysis of C(T), SEN(B), and K_T = 1 specimens via X-ray computed tomography.

Specimen	Number of detected voids	Total volume of material	Total volume of voids	Largest volume of voids	Largest radius of voids	Average Sphericity
		[mm^3]	[mm^3]	[mm^3]	[mm]	
C(T)	11,540	20,29	148.43	0.177	0.80	0.49
SEN(B)	2,853	24,12	54.36	1.451	1.60	0.55
K_T = 1	3,428	7,07	23.38	0.160	0.98	0.57

Figure 2(a) shows crack growth-rate data generated at a loading ratio of 0.1 on wrought large-crack specimens with widths of 1, 2, and 3 inches, and AM C(T) and SEN(B) specimens [10,14]. The wrought and AM samples show comparable behavior at higher rates; however, the AM samples showed significantly higher crack growth rates in the low-rate regime. In general, the AM samples showed a larger band of scatter in fatigue-crack-growth rates, especially at higher growth rates. The predicted ΔK_{eff}-rate curve, generated by the FASTRAN crack-closure model, is also shown in this figure. This model describes the data well in the low-rate region, but generally underestimates crack growth rates in the high-rate region, especially for the SEN(B) samples. Figure 2(b) shows the results of a high-R, K_{max} = 20 MPa-$m^{1/2}$ test on AM samples. This high loading ratio eliminates the effects of crack closure, resulting in higher crack growth rates. The

FASTRAN prediction curve agrees well with the data in the low crack growth region, but significantly underestimates crack growth in the high-rate, low-cycle region.

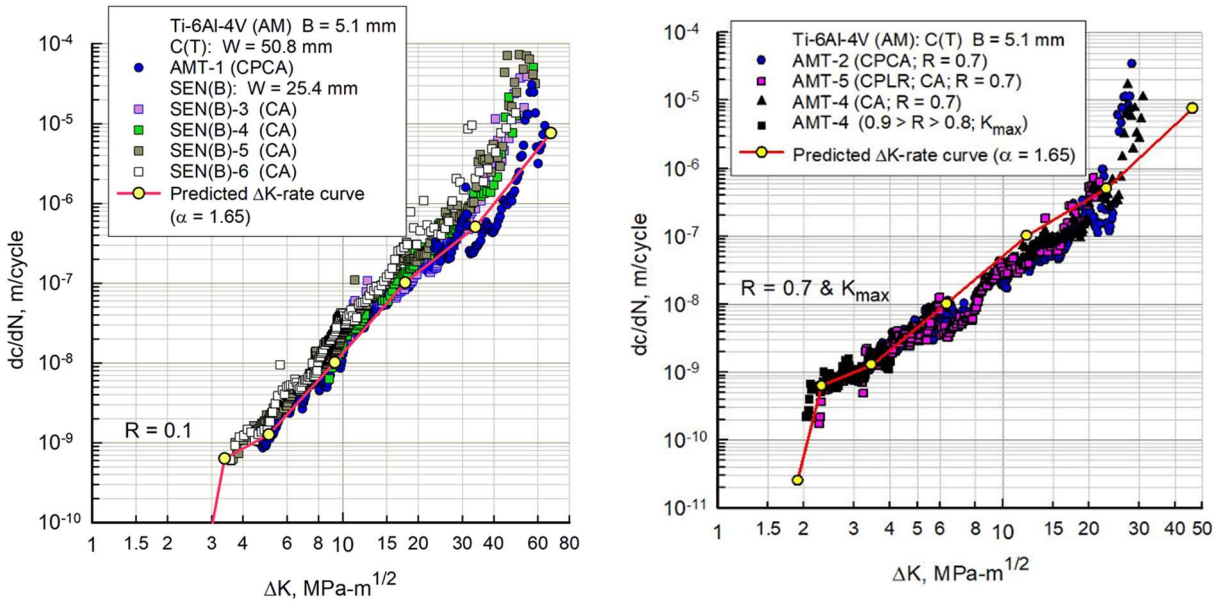

Figure 2. (a) Crack-growth-rate data for DED-LB Ti-6Al-4V (AM) and wrought Ti-6Al-4V (STOA) at R = 0.1, obtained by testing C(T) and SEN(B) specimens along with the ΔK_{eff}-rate curve for the DED-LB Ti-6Al-4V at R = 0.1; (b) Crack-growth-rate data for DED-LB Ti-6Al-4V (AM) at R = 0.7 and K_{max}, obtained by testing C(T) specimens, with the corresponding ΔK_{eff}-rate curve [10].

The FASTRAN [15] fatigue life-prediction code was used to model crack growth from an initial microstructural flaw size to failure. FASTRAN uses a plasticity-induced crack closure model based on the crack growth approach. This model accounts for the effects of plastic deformation near the crack tip. The crack-growth relation used was as follows:

$$dc/dN = C_{1i}(\Delta K_{eff})^{C_{2i}} \quad (1)$$

where C_{1i} and C_{2i} are the coefficient and exponent for each linear segment (i = 1 to n), respectively, and ΔK_{eff} is the effective stress-intensity factor.

A constant, α, is used in the FASTRAN code to shift the ΔK_{eff} baseline curve to more accurately predict the ΔK_{eff}-rate curve by increasing tensile flow stress in the plastic zone. The value of α = 1.65 was chosen to fit the DED-LB Ti-6Al-4V test data, accounting for the effects of plasticity, surface roughness, and debris buildup on the crack surfaces. Figure 3 presents the ΔK_{eff}-rate curve for DED-LB Ti-6Al-4V, depicted by solid blue lines with circular markers. Crack growth rate data for R = 0.1 are shown with solid circular markers, alongside the predicted curve for R = 0.1, represented by solid red lines and circular markers.

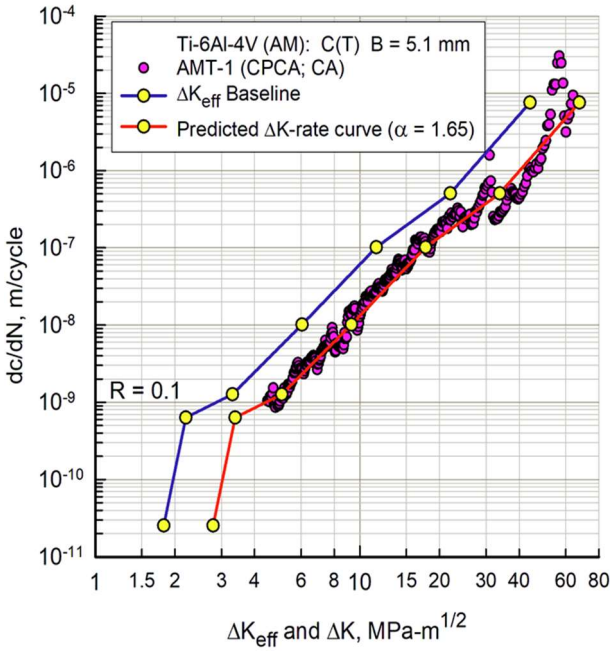

Figure 3. Effective stress-intensity factor versus crack growth rate and predicted curve for DED-LB Ti-6Al-4V (AM) at R = 0.1.

The results of the experimental fatigue testing and the FASTRAN fatigue-life predictions for the SEN(B) specimens are presented in Figure 4(a). For the fatigue modeling, an initial flaw size of 1.6 mm was used, corresponding to the largest defect identified in these specimens through X-ray computed tomography. This flaw was modeled as a surface crack located at the notch root. As shown, the simulation results closely align with the experimental data. The results of the experimental fatigue testing and FASTRAN fatigue-life predictions for DED-LB Ti-6Al-4V K_T = 1 specimens are presented in Figure 7. For these specimens, it was assumed that a corner crack would initiate fatigue failure, based on fractographic analysis of the fatigue fracture surfaces. An initial flaw size of 0.98 mm was selected, corresponding to the defect size identified through X-ray computed tomography. The predicted fatigue life under low stress levels, corresponding to the high cycle fatigue (HCF) regime, aligned well with the experimental results. However, at higher stress levels, corresponding to low cycle fatigue (LCF) and mid-life regimes, the model overestimated the fatigue life.

The overestimation at higher stress levels is attributed to the presence of numerous process-induced defects in the fatigue specimens, facilitating crack initiation at multiple locations, and the coalescence of these cracks leads to a shorter fatigue life. The interaction of stress fields between nearby large voids leads to overlapping local stress concentrations. These interacting stress fields can induce increased plastic deformation, creating multiple potential crack initiation sites. To capture the impact of multi-site crack initiation and growth under higher stress levels, fatigue modeling was extended using a multi-crack approach. The results of this multi-crack modeling for the K_T = 1 specimens are shown in Figure 4(b) as the red line. As demonstrated, the incorporation of multi-site crack growth for higher stress levels, combined with single-crack growth modeling for HCF, significantly improved the agreement with the experimental data.

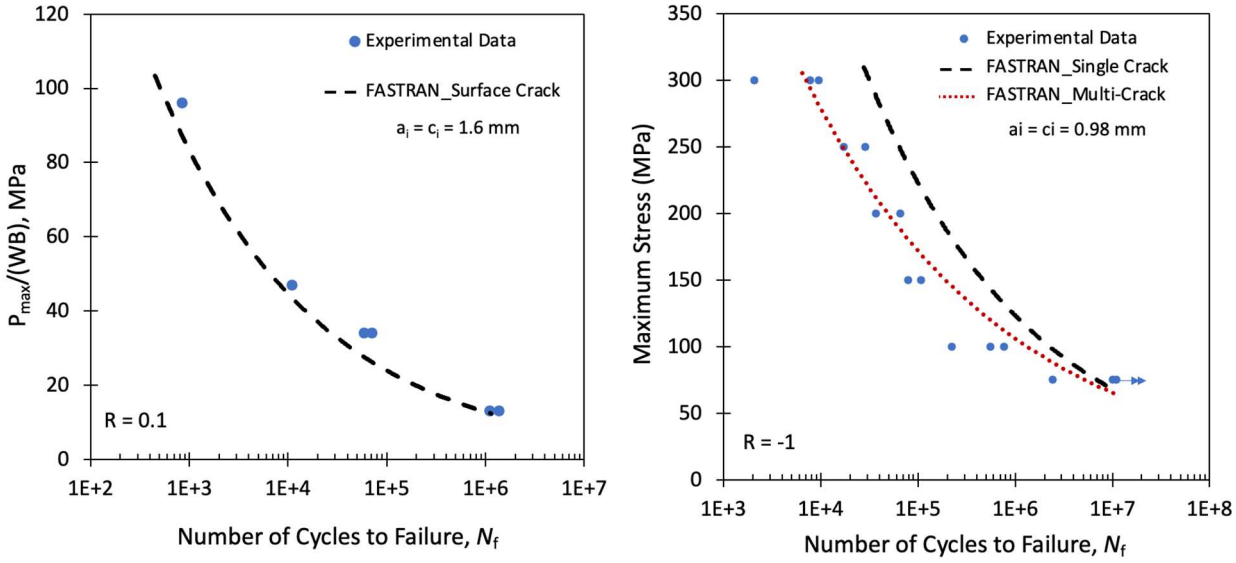

Figure 4. Experimental data and calculated fatigue curves using FASTRAN code for (a) DED-LB SEN(B) and (b) DED-LB K_T = 1 specimens.

Conclusions

In this study, the fatigue-crack-growth and fatigue-life behaviors of Ti-6Al-4V specimens fabricated via laser directed energy deposition (DED-LB) were systematically investigated and compared to their conventionally manufactured counterparts. Fatigue life predictions for both notched and unnotched specimens were generated using the FASTRAN plasticity-induced crack closure model. The results demonstrated that while the crack growth behavior of AM Ti-6Al-4V closely aligns with that of wrought Ti-6Al-4V at higher growth rates, the AM specimens exhibited significantly increased growth rates in the low-rate regime. This suggests a more complex crack propagation mechanism in AM materials, driven by process-induced defects. A key finding of this work is the necessity of incorporating multi-crack initiation and propagation mechanisms into fatigue life prediction models for AM materials. The presence of near-proximity large defects, such as LOF, inherent to the AM process, significantly affects fatigue performance. Therefore, accurately capturing the interactions between voids and the coalescence of multiple cracks is crucial, particularly in the LCF regime. Improving the accuracy of fatigue-life prediction for AM components is crucial for enhancing their reliability and facilitating their adoption in highly regulated industries such as aerospace and nuclear, where safety and performance standards are critical.

Acknowledgment

The authors acknowledge the support and laboratory resources provided by the Center for Advanced Vehicular Systems (CAVS) at Mississippi State University.

References

[1] Yadollahi A, Shamsaei N. Additive manufacturing of fatigue resistant materials: Challenges and opportunities. International Journal of Fatigue. 2017;98:14-31.
[2] Thompson SM, Bian L, Shamsaei N, Yadollahi A. An overview of Direct Laser Deposition for additive manufacturing; Part I: Transport phenomena, modeling and diagnostics. Additive Manufacturing. 2015;8:36-62.
[3] Shamsaei N, Yadollahi A, Bian L, Thompson SM. An overview of Direct Laser Deposition for additive manufacturing; Part II: Mechanical behavior, process parameter optimization and control. Additive Manufacturing. 2015;8:12-35.
[4] Gorelik M. Additive manufacturing in the context of structural integrity. International Journal of Fatigue. 2017;94:168-77.
[5] Yadollahi A, Mahmoudi M, Elwany A, Doude H, Bian L, Newman Jr JC. Effects of crack orientation and heat treatment on fatigue-crack-growth behavior of AM 17-4 PH stainless steel. Engineering Fracture Mechanics. 2020;226:106874.
[6] Riemer A, Richard HA, Brüggemann JP, Wesendahl JN. Fatigue crack growth in additive manufactured products. Frattura ed Integrità Strutturale. 2015;9.
[7] Zhai Y, Lados DA, Brown EJ, Vigilante GN. Fatigue crack growth behavior and microstructural mechanisms in Ti-6Al-4V manufactured by laser engineered net shaping. Int J Fatigue. 2016;93:51-63.
[8] Gallagher JP, van Stone RH, deLaneuville RE, Gravett P, Bellows RS. Improved High-Cycle Fatigue (HCF) Life Prediction. AFRL-ML-WP-TR; 2001. p. 05515.
[9] Nguyen HD, Pramanik A, Basak AK, Dong Y, Prakash C, Debnath S, Shankar S, Jawahir IS, Dixit S, Buddhi D. A critical review on additive manufacturing of Ti-6Al-4V alloy: Microstructure and mechanical properties. Journal of Materials Research and Technology. 2022;18:4641-61.
[10] Yadollahi A, Buiter L, Mahtabi MJ, Doude HR, Rhee H, Newman Jr JC. Fatigue Life and Crack Growth Behavior of Ti-6Al-4V Fabricated via Laser Directed Energy Deposition. Materials Performance and Characterization. 2024;13(2).
[11] ASTM E466-07. Standard Practice for Conducting Force Controlled Constant Amplitude Axial Fatigue Tests of Metallic Materials, 2007.
[12] ASTM E647-15, Standard test method for measurement of fatigue crack growth rates, 2015.
[13] Newman Jr JC, Yamada Y, Ziegler BM, Shaw JW. Small-and large-crack databases for rotorcraft materials. DOT/FAA/AR-12; 2012.
[14] Newman Jr. JC, Kota K, Lacy TE. Fatigue and crack-growth behavior in a titanium alloy under constant-amplitude and spectrum loading. Engineering Fracture Mechanics. 2018;187:211-24.
[15] Newman Jr JC. FASTRAN—A fatigue crack growth life prediction code based on the crack-closure concept. Version 54 User Guid Fatigue Fract Assoc LLC, Eupora, MS. 2012.